International Journal of Scientific Research in Engineering and Management (IJSREM)
Volume: 10 Issue: 04 | April - 2026 SJIF Rating: 8.659 ISSN: 2582-3930

Plant-Mediated Synthesis of TiO_2 Nanoparticles: Comparative Study of Structural, Antibacterial, and Anticorrosive Properties

J. Maria Agnes Preethi[1], Ms. D. Carolin Jeniba Rachel[2]

[1]II M.Sc Chemistry PG Department of Chemistry, St. Mary's College (Autonomous) Thoothukudi–628001.

[2]Assistant Professor, PG Department of Chemistry, St. Mary's College (Autonomous) Thoothukudi–628001.

Abstract

This study reports the green synthesis of titanium dioxide (TiO_2) nanoparticles using *Monoon longifolium* leaf extract and a comparative evaluation of two synthesis approaches, namely ultrasonication (TiO-A) and magnetic stirring (TiO-B). The formation and physicochemical properties of the nanoparticles were confirmed through UV–Visible spectroscopy, FTIR, XRD, FESEM, EDX, and TGA analyses, revealing nanoscale crystalline structures with effective surface functionalization by plant-derived biomolecules. Optical studies indicated characteristic UV absorption, while XRD confirmed phase purity and nanocrystalline nature. Morphological and elemental analyses further validated the successful formation of TiO_2 nanoparticles. The antibacterial activity demonstrated moderate efficacy against both Gram-positive and Gram-negative bacteria, with TiO-A showing comparatively higher inhibition due to improved surface characteristics. Additionally, anticorrosion studies using the weight-loss method revealed that nanoparticle-coated mild steel exhibited reduced corrosion rates in acidic, basic, and neutral media, with maximum protection observed under neutral conditions. The enhanced performance is attributed to the formation of a stable protective layer and effective surface coverage by nanoparticles. Overall, the findings highlight that plant-mediated TiO_2 nanoparticles, particularly TiO-A, possess promising antibacterial and anticorrosive properties, making them suitable for biomedical and environmental applications.

Key Words: Green synthesis, Titanium dioxide nanoparticles (TiO_2 NPs), *Monoon longifolium*, Ultrasonication, Magnetic stirring, Phytochemical reduction.

1.INTRODUCTION

Titanium dioxide (TiO_2), also referred to as titanium (IV) oxide or titania, is an inorganic compound widely recognized for its stability and versatility [1]. It appears as a white, odourless solid that is insoluble in water, although certain naturally occurring forms may exhibit darker coloration. Due to its high refractive index and excellent light-scattering ability, TiO_2 is extensively employed as a white pigment in paints, coatings, plastics, and cosmetic formulations [2]. The compound possesses a density of 4.23 g/cm³ and a molar mass of 79.866 g/mol, along with notable thermal stability characterized by a melting point of 1843°C and a boiling point of 2972°C. In addition to its pigment applications, titanium dioxide is used as a food additive in products such as confectionery and dairy items. It also plays a significant role in thin-film coatings, where it enhances optical reflectivity and produces decorative effects. Furthermore, nanoscale TiO_2 is widely utilized in sunscreens and skincare products as an effective UV-blocking agent, offering protection against both UV-A and UV-B radiation while maintaining chemical stability and low toxicity.

2. Materials and Methods

Collection of Plants

Fresh leaves of *Monoon longifolium* were obtained from St. Mary's College (Autonomous), Thoothukudi. The leaves were thoroughly cleaned using running tap water to eliminate dust and surface impurities, followed by a rinse with distilled water. Subsequently, the washed leaves were shade-dried at ambient temperature for approximately seven days to preserve heat-sensitive bioactive constituents. After complete drying, the leaves were stored in clean, airtight containers for further preparation of the plant extract.

Preparation of Leaf Extract

The shade-dried leaves of *Monoon longifolium* were ground into a fine powder using a blender and kept in airtight containers at room temperature. Approximately 10 g of the powdered leaf sample was placed in a clean beaker containing 150 mL of distilled water. The mixture was then heated at 60–80 °C for about 40 minutes with constant stirring to facilitate the extraction of bioactive compounds. After heating, the solution was allowed to cool to room temperature and

subsequently filtered using Whatman No. 1 filter paper. The obtained clear filtrate served as the aqueous leaf extract and was preserved at 4 °C for further use in nanoparticle synthesis.

Synthesis of Titanium Oxide nanoparticles using Ultra Sonicator

Titanium oxide nanoparticles were synthesized by adding 10 mL of titanium isopropoxide to the *Monoon longifolium* leaf extract under continuous ultrasonication. The reaction mixture was maintained at approximately 30 °C for 4 hours. The formation of nanoparticles was indicated by a visible colour change from pale yellow to dark yellow along with the appearance of turbidity, suggesting the reduction of titanium ions and the generation of TiO precursor species facilitated by phytochemicals in the extract. Upon completion of the reaction, the mixture was cooled to room temperature and filtered using Whatman No. 1 filter paper. The resulting filtrate was dried in a hot air oven to remove moisture completely. The dried material was then subjected to calcination in a muffle furnace at 500–550 °C for 3–4 hours to obtain titanium oxide nanoparticles. The synthesized sample, designated as TiO-A, was collected and stored in airtight containers for further characterization and application studies.

Synthesis of Titanium Oxide Nanoparticles using Magnetic Stirrer

Titanium oxide nanoparticles were prepared by introducing 10 mL of titanium isopropoxide into the *Monoon longifolium* leaf extract under continuous magnetic stirring. The reaction mixture was maintained at 60 °C for 1 hour. The progression of the reaction was indicated by a noticeable colour change from pale yellow to dark yellow along with the development of turbidity, confirming the reduction of titanium ions and the formation of TiO precursor complexes mediated by phytochemicals present in the extract. After completion, the reaction mixture was allowed to cool to room temperature and then filtered using Whatman No. 1 filter paper. The collected filtrate was dried in a hot air oven to ensure complete removal of moisture. The resulting dried material was calcined in a muffle furnace at 500–550 °C for 3–4 hours to obtain titanium oxide nanoparticles. The synthesized sample was labeled as TiO-B, collected, and stored in airtight containers for further characterization and application studies.

Results and Discussions

UV–Visible Spectroscopy

UV–Visible Spectroscopy of TiO-A & TiO-B Nanoparticles

The optical properties of the green-synthesized TiO-A and TiO-B nanoparticles were systematically investigated using UV–Visible absorption spectroscopy (Figure-1). Both samples exhibited strong absorption in the ultraviolet region, confirming the successful formation of nanoscale TiO_2. TiO-A nanoparticles showed a prominent absorption band in the range of 291–329 nm, while TiO-B nanoparticles displayed distinct peaks at approximately 259 nm and 346 nm. These absorption features are characteristic of intrinsic electronic transitions from the valence band to the conduction band of TiO_2 nanoparticles, which is a well-established signature of their formation [3]. The absorption edge observed near 346 nm for TiO-B corresponds to the fundamental band gap transition, whereas the additional peak around 259 nm may be attributed to surface defect states, excitonic transitions, or the influence of phytochemical constituents acting as reducing, capping, and stabilizing agents during the green synthesis process [7,8]. In comparison with previously reported studies, green-synthesized TiO_2 nanoparticles typically exhibit absorption in the range of 300–400 nm depending on synthesis conditions and the nature of the biological extract used [4,5,9,10]. The observed blue shift in the TiO-A absorption band suggests reduced particle size and possible quantum confinement effects, indicating finer nanoparticle formation. Furthermore, the absence of significant absorption in the visible region for both samples confirms their high purity and minimal aggregation, while the relatively sharp absorption edges indicate good crystallinity and a narrow particle size distribution, consistent with earlier reports on bioinspired metal oxide nanoparticles [11,3].

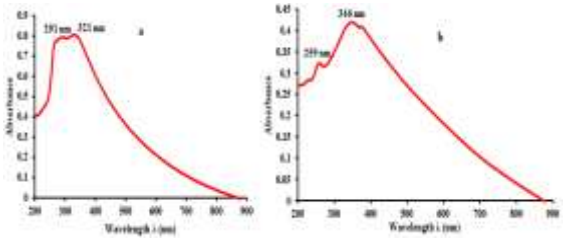

Figure – 1: UV-Visible absorption spectrum of TiO-A & TiO-B nanoparticles

Fourier Transform Infrared Spectroscopy (FTIR)

FT-IR Spectroscopy of TiO-A & TiO-B Nanoparticles

Fourier Transform Infrared (FT-IR) spectroscopy was employed to elucidate the functional groups involved in the reduction and stabilization of both TiO-A and TiO-B nanoparticles synthesized via the green route (Figure-2). The FT-IR spectra of both samples exhibited broad and intense absorption bands in the high wavenumber region, with TiO-A showing peaks at 3911.64 cm^{-1} and 3657.04 cm^{-1}, and TiO-B displaying a prominent band at 3471 cm^{-1}, all of which are attributed to O–H stretching vibrations of hydroxyl groups arising from surface-adsorbed water molecules and phytochemical constituents present in the plant extract [3–5,10,12]. The appearance of bands at 2939 cm^{-1} in TiO-B and 1543.05 cm^{-1} in TiO-A corresponds to C–H stretching and O–H bending vibrations, respectively, indicating the presence of residual organic moieties that originate from biomolecules acting as reducing and capping agents during synthesis [5,9,13,14–16]. Additionally, the absorption band at 1651 cm^{-1} observed in TiO-B is associated with H–O–H bending vibrations, further confirming the presence of molecularly adsorbed water and surface hydroxylation [4,10,12]. The most significant features for both samples are the strong absorption bands in the lower wavenumber region, where TiO-A exhibits peaks at 686.86 cm^{-1}, 648.68 cm^{-1}, 595.47 cm^{-1}, 547.78 cm^{-1}, and 493.78 cm^{-1}, while TiO-B shows bands at 686 cm^{-1}, 601 cm^{-1}, and 432 cm^{-1}. These bands are characteristic of Ti–O, Ti–O–Ti, and O–Ti–O lattice vibrations, confirming the successful formation of the titanium dioxide crystalline framework. The dominance of absorption peaks below 700 cm^{-1} is a well-known fingerprint of TiO_2 nanostructures and is consistent with previously reported studies on green-synthesized titanium dioxide nanoparticles using various biological extracts.

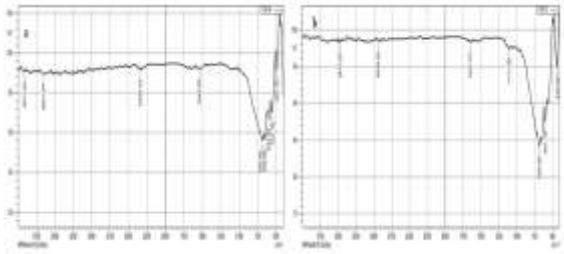

Figure – 2: FT-IR spectrum of TiO-A & TiO-B nanoparticles

X-Ray Diffraction Studies

XRD Studies of TiO – A & TiO-B nanoparticles

The X-ray diffraction (XRD) patterns of the green-synthesized TiO-A and TiO-B nanoparticles (Figure-3) confirm their crystalline nature and phase purity. In the case of TiO-A, distinct and sharp diffraction peaks were observed at 2θ values of approximately 25.5°, 37.8°, 48.0°, 54.2°, 55.3°, 62.9°, 70.3°, and 75.3°, which are indexed to the (101), (004), (200), (105), (211), (204), (220), and (215) crystallographic planes of TiO_2 (JCPDS card No. 96-152-6932) [17]. These characteristic reflections confirm the formation of a highly crystalline TiO-A phase, consistent with earlier reports on green-synthesized TiO_2 nanoparticles [3,5,6]. The absence of additional peaks corresponding to rutile, brookite, or other impurity phases indicates high phase purity. The average crystallite size, estimated using the Debye–Scherrer equation, falls within the nanoscale range (20–40 nm), while the calculated average crystallite size (D) is 7.7 nm, further confirming the nanocrystalline nature of the material [14,15]. Similarly, the XRD pattern of TiO-B nanoparticles exhibits well-defined diffraction peaks at 2θ values of approximately 25.3°, 28.6°, 48.6°, 54.3°, 55.4°, 62.1°, 69.0°, and 75.1°, corresponding to the (110), (002), (020), (112), (022), (113), (023), and (311) planes of the monoclinic TiO-B phase (JCPDS card No. 96-153-0152) [17]. The presence of these peaks confirms the successful formation of the TiO-B polymorph, which is structurally distinct from anatase and rutile phases. The absence of secondary phase peaks further indicates good phase purity, while the sharp and intense diffraction peaks suggest good crystallinity despite the metastable nature of TiO-B. The average crystallite size calculated using the Debye–Scherrer equation is in the range of 20–40 nm, with an average value (D) of 8.95 nm, confirming nanoscale dimensions and uniform particle distribution, in agreement with previously reported studies.

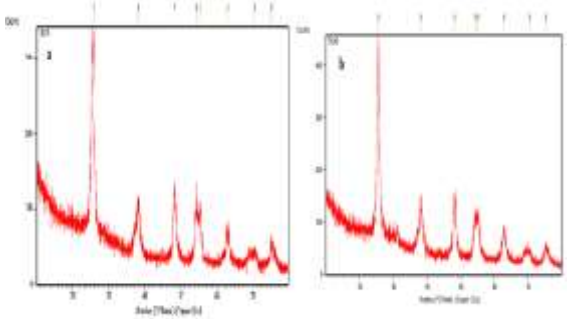

Figure – 3: XRD spectrum of TiO-A & TiO-B nanoparticles

Field Emission Scanning Electron Microscopy (FESEM)

FESEM of TiO-A & TiO-B nanoparticles

The FESEM images of the green-synthesized TiO-A and TiO-B (Figure-4) nanoparticles reveal densely packed, highly agglomerated structures composed of quasi-spherical to irregular nanosized particles with uniform distribution. The TiO-B nanoparticles exhibit relatively more compact clustering and defined grain boundaries compared to TiO-A, indicating stronger interparticle interactions. In both cases, the particle sizes observed are in the nanometer range and are consistent with XRD results, confirming successful nanoscale formation. The rough and porous surface morphology suggests the effective role of phytochemicals in reduction and stabilization during green synthesis. Such agglomerated and textured nanostructures are characteristic of plant-mediated metal oxide nanoparticles due to high surface energy and limited capping, aligning well with previous reports [18, 19, 11, 20].

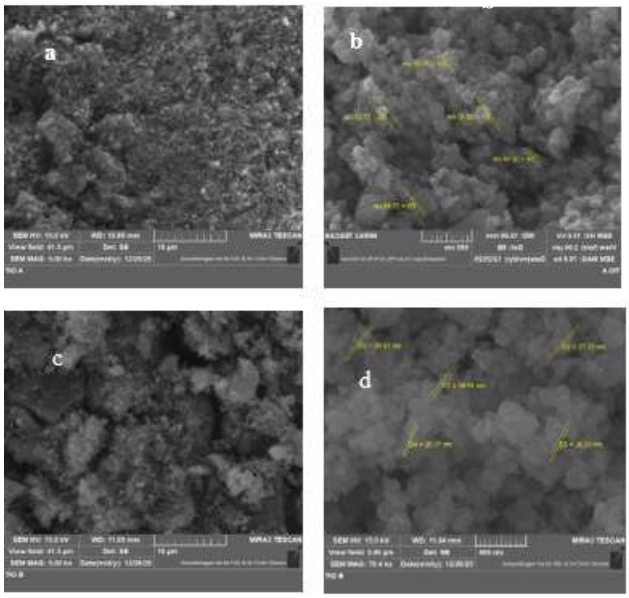

Figure – 4: FESEM images of TiO-A & TiO-B in different maginfication a & c) 10 μm b & d) 500nm

Energy Dispersive X-Ray Analysis

EDX Analysis of TiO-A & TiO-B nanoparticles

Energy Dispersive X-ray (EDX) analysis of both TiO-A and TiO-B (Figure-5) nanoparticles confirms the successful formation of titanium dioxide through the dominant presence of titanium (Ti) and oxygen (O) as major elements, while the detection of a minor potassium (K) signal is attributed to residual plant-derived biomolecules involved in the green synthesis process; such elemental profiles are consistent with previously reported plant-mediated metal oxide nanoparticles, thereby validating the purity and biogenic origin of the synthesized TiO_2 nanoparticles [18, 19, 11, 20].

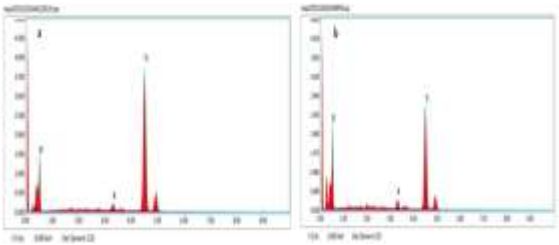

Figure – 5: EDAX spectrum of TiO-A & TiO-B nanoparticles

Table – 1: Elemental composition of TiO-A & TiO-B nanoparticles

Sample	Element	Weight %	Atomic %
TiO-A	Ti	68.51	43.01
	O	29.51	55.47
	K	1.98	1.52
TiO-B	Ti	55.81	30.53
	O	41.17	67.44
	K	3.02	2.03

Thermogravimetric Analysis

Thermogravimetric Analysis of TiO-A & TiO-B nanoparticles

Thermogravimetric analysis (TGA) and combined DTA–DTG profiles of the green-synthesized TiO-A and TiO-B (Figure-6) nanoparticles reveal a multistep weight loss pattern associated with moisture evaporation, decomposition of organic phytoconstituents, and subsequent stabilization of the TiO_2 framework; the initial weight loss below 200 °C corresponds to the removal of physically adsorbed water, followed by a major loss between 200–500 °C due to the decomposition of bioactive molecules involved in reduction and capping, while the minimal weight change at higher temperatures indicates the formation of thermally stable TiO_2 nanoparticles, with TiO-B exhibiting comparatively higher residue and slightly enhanced thermal stability due to denser aggregation and stronger interparticle interactions, consistent with previously reported behavior of plant-mediated metal oxide nanoparticles [18, 19, 11, 20].

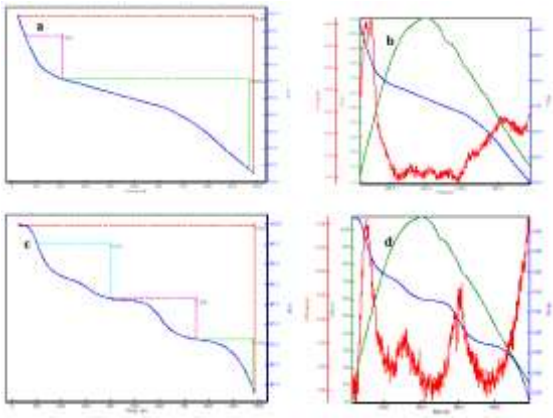

Figure – 6: TGA Analysis of TiO-A & TiO-B nanoparticles

Antibacterial Activity

The antibacterial efficacy of green-synthesized TiO-A and TiO-B nanoparticles (Figure-7) was assessed by the agar well diffusion method against *Escherichia coli*, *Staphylococcus aureus*, *Bacillus subtilis*, *Bacillus cereus*, and *Klebsiella pneumoniae*, using ciprofloxacin as a positive control. The standard drug exhibited pronounced inhibition zones (25–30 mm), validating the assay conditions, whereas both nanoparticle systems demonstrated moderate yet distinct antibacterial activity. TiO-A showed relatively higher efficacy with inhibition zones ranging from 9–14 mm, displaying maximum activity against *Bacillus cereus* (14 mm) and *E. coli* (13 mm), followed by *Staphylococcus aureus* (11 mm) and *Klebsiella pneumoniae* (9 mm), while no inhibition was observed against *Bacillus subtilis*. In contrast, TiO-B exhibited comparatively lower activity (6–10 mm), with notable inhibition against *Staphylococcus aureus* and *Klebsiella pneumoniae* (10 mm), and reduced effectiveness toward *E. coli* and *Bacillus cereus* (6 mm), with no activity against *Bacillus subtilis*. The superior performance of TiO-A can be attributed to differences in physicochemical characteristics such as reduced particle size, enhanced surface area, and improved surface functionalization arising from plant-mediated synthesis, which facilitate stronger interaction with microbial cells. Furthermore, Gram-positive bacteria showed relatively higher susceptibility than Gram-negative strains due to the absence of an outer lipopolysaccharide barrier, enabling easier nanoparticle penetration. Similar antibacterial trends have been reported for plant-derived TiO_2 nanoparticles, where synthesis conditions significantly influence biological activity and surface reactivity [3–5,9,21,12,22]. Although the inhibition zones were smaller than the standard antibiotic, the results confirm that both TiO-A and TiO-B nanoparticles possess appreciable antibacterial potential, supporting their applicability in biomedical and environmental antimicrobial systems.

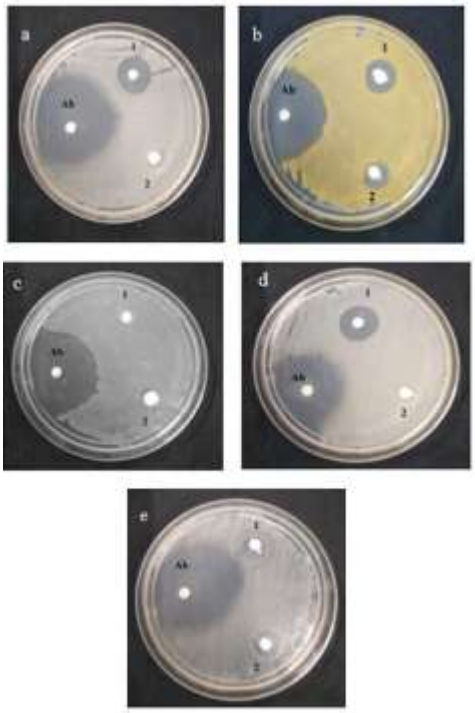

Figure – 7: Antibacterial activity of a) *Escherichia coli,* b) *Staphylococcus aureus,* c) *Bacillus subtilis, d) Bacillus cereus, e) Kleibsiella pneumonia* TiO-A and TiO-B nanoparticles

Table – 2: Antibacterial activity of TiO-A & TiO-B nanoparticles

Bacteria	**Inhibition zone in mm**		
	Ab ciprofloxacin	**1-TiO-A**	**2-TiO-B**
Escherichia coli	30	13	6
Staphylococcus aureus	30	11	10
Bacillus subtilis	30	-	-
Bacillus cereus	25	14	6
Kleibsiella pneumonia	30	9	10

Anti-corrosion Activity

The anticorrosion performance of green-synthesized TiO-A and TiO-B nanoparticle coatings was assessed using the weight-loss method in acidic, basic, and neutral media over a 9-day immersion period, revealing

a consistent reduction in metal deterioration compared to uncoated samples. The coated specimens exhibited lower weight loss values (0.1147 g in acidic, 0.1714 g in basic, and 0.0542 g in neutral media) relative to the uncoated metal (0.101 g, 0.1529 g, and 0.0453 g, respectively), indicating the formation of a protective barrier layer on the metal surface.

Table – 3: Corrosion rate % without TiO-A and TiO-B nanoparticles

Without TiO-A and TiO-B	Wi (g)	Wf (g)	ΔW (g)	Corrosion rate%
Acid	7.6784	7.5637	0.1147	1.49
Base	7.6729	7.5015	0.1714	2.23
Neutral	7.6853	7.6311	0.0542	0.70

The calculated inhibition efficiencies were approximately 14.6% in acidic, 13.1% in basic, and 20.6% in neutral media, with the highest protection observed under neutral conditions, suggesting enhanced coating stability and reduced electrochemical interaction in less aggressive environments. The improved corrosion resistance is attributed to the uniform surface coverage, strong adhesion, and inherent chemical stability of TiO_2 nanoparticles, which limit the penetration of corrosive species and suppress anodic–cathodic reactions at the metal interface. Although moderate variations in corrosion rates were observed across different media, the overall trend confirms that TiO-A exhibited comparatively better protective behavior than TiO-B, likely due to differences in particle characteristics such as surface area and compactness of the oxide layer. These findings are consistent with earlier reports on plant-mediated TiO_2 nanoparticle coatings demonstrating effective anticorrosion performance through barrier formation and surface passivation mechanisms [3–5,23].

Table – 4: Corrosion rate % of with TiO-A nanoparticles

Medium	Wi (g)	Wf (g)	Corrosion rate %
Acid	7.7224	7.6214	1.30
Base	7.7599	7.6070	1.97
Neutral	7.7203	7.6750	0.58

Table – 5: Corrosion rate % with TiO-B nanoparticles

Medium	Wi (g)	Wf (g)	Corrosion rate %
Acid	7.7152	7.6954	0.25
Base	7.7124	7.6732	0.50
Neutral	7.7200	7.6836	0.47

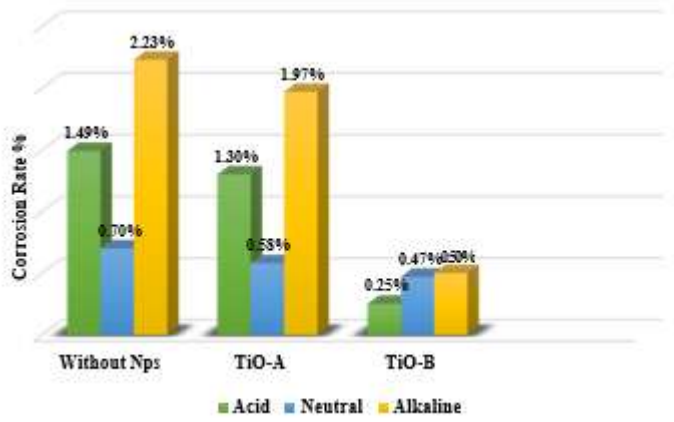

Figure – 8: Corrosion rate % of TiO-A & TiO-B nanoparticles

Table - 6: Anticorrosion activity % of TiO-A nanoparticles

Without nanoparticle	With nanoparticle	Anti corrosion %
1.49	1.30	12.7
2.23	1.97	11.6
0.70	0.58	17.1

Table – 7: Anticorrosion activity % of TiO-B nanoparticles

Without nanoparticle	With nanoparticle	Anticorrosion %
1.49	0.25	83.2
2.23	0.50	77.5
0.70	0.47	32.8

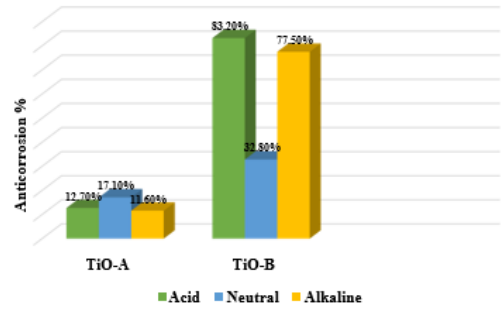

Figure – 9: Anticorrosion rate % of TiO-A & TiO-B nanoparticles

3. CONCLUSIONS

Titanium dioxide nanoparticles were successfully synthesized by a green, simple, and cost- effective method using *Monoon longifolium* leaf extract. Two samples, TiO-A and TiO-B, were prepared and systematically characterized using UV–Visible spectroscopy, FT-IR, XRD, SEM, EDAX, TGA, TG–DTG–DTA, antibacterial and anti-corrosion.

- From UV–Visible spectroscopy, both TiO-A and TiO-B confirmed nanoparticle formation through characteristic UV absorption; however, TiO-A exhibited a blue shift, indicating smaller particle size and enhanced quantum confinement compared to TiO-B.
- The FTIR analysis of both samples confirmed the presence of phytochemical functional groups responsible for reduction and stabilization. TiO-A showed relatively stronger interaction with biomolecules, suggesting better surface functionalization than TiO-B.
- XRD studies revealed that both nanoparticles are highly crystalline and phase-pure. TiO-A predominantly exhibited anatase phase characteristics with smaller crystallite size (~7.7 nm), whereas TiO-B showed a distinct polymorphic structure with slightly larger crystallite size (~8.95 nm), indicating that synthesis method influences crystal phase and size.
- From FESEM analysis, both samples showed nanoscale agglomerated morphology, but TiO-B exhibited more compact and dense structures, while TiO-A displayed comparatively finer and less aggregated particles, contributing to higher surface area.
- EDX analysis confirmed the elemental purity of both nanoparticles with dominant Ti and O peaks. The minor presence of potassium indicated residual plant-derived compounds, validating the green synthesis approach in both cases.
- The TGA results demonstrated that both TiO-A and TiO-B possess good thermal stability, with TiO-B showing slightly higher thermal resistance due to stronger particle aggregation and compact structure.
- In terms of antibacterial activity, both nanoparticles exhibited moderate efficacy against tested microorganisms. However, TiO-A showed comparatively higher inhibition zones, which can be attributed to its smaller particle size, higher surface area, and improved interaction with bacterial cells.
- The anticorrosion studies indicated that both TiO-A and TiO-B coatings effectively reduced corrosion rates in acidic, basic, and neutral media. TiO-A demonstrated better overall protective efficiency due to uniform surface coverage and enhanced film formation, while TiO-B showed notable performance in specific conditions due to its compact structure.

Overall, the comparative analysis clearly indicates that ultrasonication (TiO-A) is a more effective synthesis method than magnetic stirring (TiO-B) in producing TiO_2 nanoparticles with superior surface properties, enhanced antibacterial activity, and better anticorrosion performance. The study highlights the potential of plant-mediated TiO_2 nanoparticles as eco-friendly materials for applications in biomedical, environmental, and corrosion protection fields.

ACKNOWLEDGEMENT

I would like to express my gratitude to my primary supervisor, Ms. D. Carolin Jeniba Rachel, who guided me throughout this project. I would also like to thank my friends and family who supported me and offered deep insight into the study.

REFERENCES

1. Völz, Hans G., et al.: "Pigments, Inorganic". *Ullmann's Encyclopedia of Industrial Chemistry*. Weinheim: Wiley-VCH. (2006).

2. Hanaor DA, Xu W, Ferry M, Sorrell CC.: "Abnormal grain growth of rutile TiO2 induced by ZrSiO4". *Journal of Crystal Growth*. (2012). 83–91.

3. Vishal Verma, Mawaheb Al-Dossari, Jagpreet Singh, et al.: A Review on Green Synthesis of TiO2 NPSs: Photocatalysis and Antimicrobial Applications. Polymers, (2022). 14, 1444.

4. Abel Saka, Yohannes Shifera, Leta Tesfaye Jule, et al.: Biosynthesis of TiO2 nanoparticles by Caricaceae (Papaya) shell extracts for antifungal application. Scientific Reports, (2022). 12.

5. Afzal Ansari, Vasi Uddin Siddiqui, Wahid UlRehman, et al.: Green Synthesis of TiO2 Nanoparticles Using Acorus calamus Leaf Extract and Evaluating Its Photocatalytic and In Vitro Antimicrobial Activity. Catalysts, (2022). 12, 181.

6. Abouelkacem SAHRAOUI, Mouna HAMLAOUI, Sara CHIKHI, et al.: Green synthesis and characterization of titanium dioxide nanoparticles using Eucalyptus globulus leaf extract: Impacts of the mild thermal treatment. Materials Today Sustainability, (2025). 31.

7. Kalpana, V.N.; Devi Rajeswari, V.: A Review on Green Synthesis, Biomedical Applications, and Toxicity Studies of ZnO NPSs. Bioinorg. Chem. Appl. (2018).

8. Bahrulolum, H.; Nooraei, S.; Javanshir, N.; Tarrahimofrad, H.; Mirbagheri, V.S.; Easton, A.J.; Ahmadian, G.: Green synthesis of metal nanoparticles using microorganisms and their application in the agrifood sector. J. Nanobiotechnol. (2021). 19, 86.

9. Devipriya Anbumani, Kayal vizhi Dhandapani, Janani Manoharan et al.: Green synthesis and antimicrobial efficacy of titanium dioxide nanoparticles using Luffa acutangular leaf extract. Journal of King Saud University - Science. (2022). 34.

10. S. Shanavas, A. Priyadharsan, S. Karthikeyan et al.: Green synthesis of titanium dioxide nanoparticles using *Phyllanthus niruri* leaf extract and study on its structural, optical and morphological properties. Materialstoday. (2020). 26.

11. Chouke, P.B.; Shrirame, T.; Potbhare, et al.: Bioinspired metal/metal oxide nanoparticles: A road map to potential applications. *Mater. Today Adv.* (2022). *16*.

12. V. Devi Rajeswari, Emad M. Eed, Ashraf Elfasakhany, et al.: Green synthesis of titanium dioxide nanoparticles using *Laurus nobilis* (bay leaf): antioxidant and antimicrobial activities. Applied Nanoscience. (2023), 13, 1477–1484.

13. Hedaiat Moradpoor, Mohsen Safaei, Amin Golshah, et al.: Green synthesis and antifungal effect of titanium dioxide nanoparticles on oral *Candida albicans* pathogen. Inorganic Chemistry Communications. (2021). 130.

14. S. Pavithra, T.C. Bessy, M.R. Bindhu, et al.: Photocatalytic and photovoltaic applications of green synthesized titanium oxide (TiO2) nanoparticles by Calotropis gigantea extract. Journal of Alloys and Compounds. (2023). 960.

15. Ravi Saini and Pradeep Kumar.: Green synthesis of TiO2 nanoparticles using *Tinospora cordifolia* plant extract & its potential application for photocatalysis and antibacterial activity. Inorganic Chemistry Communications. (2023). 156.

16. Shashank Shekhar, Santosh Singh, Namita Gandhi, et al.: Green chemistry based benign approach for the synthesis of titanium oxide nanoparticles using extracts of *Azadirachta Indica.* Cleaner Engineering and Technology. (2023). 13.

17. Weirich T.E., Winterer M., Seifried S., Fuess H., Hahn H., "Rietveld analysis of electron powder diffraction data fromnanocrystalline anatase, Ti O2", Ultramicroscopy **81**, (2000) 263- 270.

18. O.J. Nava, P.A. Luque, C.M. Go´mez-Gutie´rrez, et al.: Influence of camellia sinensis extract on zinc oxide nanoparticle green synthesis, J. Mol. Struc. (2017). 121-125.

19. P. Jamdagni, P. Khatri, J.S. Rana.: Green synthesis of zinc oxide nanoparticles using flower extract of Nyctanthes arbor-tristis and their antifungal activity, J. King Saud Univ.—Sci. (2016). 168-175.

20. Ijaz, I.; Bukhari, A.; Gilani, E.; Nazir, A.; Zain, H.; Saeed, R.; Hussain, S.; Hussain, T.; Bukhari, A.; Naseer, Y.; et al.: Green synthesis of silver nanoparticles using different plants parts and biological organisms, characterization and antibacterial activity. Environ. Nanotechnol. Monit. Manag. (2022). 18.

21. B.K. Thakur, A. Kumar, D. Kumar.: Green synthesis of titanium dioxide nanoparticles using *Azadirachta indica* leaf extract and evaluation of their antibacterial activity. South African Journal of Botany. (2019). 124.

22. Taqwa Ghalib Hamad, Taghried Ali Salman.: Green synthesis of titanium oxide nanoparticles using pomegranate leaf extract: Characterization and antibacterial activity evaluation. AIP Publishing. (2024).

23. Mayank Bundele Nitin Rane, Vikramaditya Lande, et al.: Green synthesis of TiO_2 nanoparticle from *Plumeria rubra* L. leaves for anticorrosion application. Materialstoday. (2023). 1685-1691.